Proceedings of the 9th International Workshop on Ship and Marine Hydrodynamics, 26 – 28 August 2015, Glasgow, UK

CFD Simulation of Vortex-Induced Vibration of a Vertical Riser

Enhao Wang, Qing Xiao[1], Atilla Incecik

Department of Naval Architecture, Ocean and Marine Engineering, University of Strathclyde, Glasgow G4 0LZ, UK

Abstract: Three-dimensional fluid-structure interaction (FSI) simulations are conducted on a vertical riser with a length-to-diameter ratio *L/D* = 481.5. Important vortex-induced vibration (VIV) parameters including the amplitude responses, orbital trajectories, oscillation frequencies and vorticity contours are presented. The computational fluid dynamics (CFD) simulation results are in good agreement with published experimental data. The riser exhibits a dual-resonant response. Two different vortex shedding mode is observed, i.e., 2P and 2S modes. 2P mode is associated with the maximum transverse amplitude and 2S mode is observed elsewhere along the riser.

Keywords: vortex-induced vibration (VIV), Computational Fluid Dynamics (CFD), fluid-structure interaction (FSI), vertical risers, uniform flow

1. Introduction

Vortex-induced vibration (VIV) is a major cause of fatigue failure in offshore slender structures. The reliable estimation of the fatigue damage of risers and mooring lines requires detailed understanding and efficient prediction of these self-excitation and self-sustained oscillations.

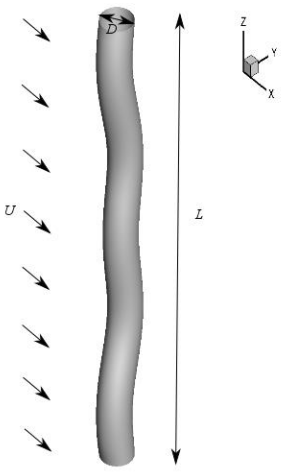

Fig. 1 Sketch of the physical configuration.

Over the past few decades, VIV has been extensively studied. For detailed information, one may refer to the review papers by Sarpkaya (1979), Bearman (1984), Williamson and Govardhan (2004), Gabbai and Benaroya (2005) and more recently by Bearman (2011).

As riser pipes often possess a high length-to-diameter ratio (*L/D*) of the order of 10^3 (Chaplin et al., 2005), many VIV experiments have been carried out on deepwater risers with high *L/D* (Chaplin et al., 2005; Gu et al., 2013; Tognarelli et al., 2004; Tognarelli et al., 2008; Trim et al., 2005; Vandiver et al., 2006).

Apart from the various experimental investigations, there have been several CFD studies on VIV of flexible cylinders with high *L/D* during the past few years. Willden and Graham (2001) used a quasi-three-dimensional numerical method to simulate an *L/D* = 100 cylinder subject to a sheared inflow. Meneghini et al. (2004) and Yamamoto et al. (2004) presented the numerical simulations of long marine risers with *L/D* up to 4600 using two-dimensional discrete vortex method (DVM). Menter et al. (2006) and Holmes et al. (2006) first simulated riser VIV using fully 3D finite volume method (FVM) and finite element method (FEM), respectively. Constantinides and Oakley (2008a; 2008b) presented the numerical simulations of long

[1] **Corresponding author email: qing.xiao@strath.ac.uk**

cylinders with *L/D* = 4200. Huang et al. (2009) performed finite-analytic Navier-Stokes (FANS) simulations on an *L/D* = 482 cylinder. Nevertheless, three-dimensional, fully coupled fluid-structure interaction (FSI) simulations of VIV of vertical risers are still quite limited. In this paper, a three-dimensional, fully coupled approach is used to study the riser VIV response in uniform currents and in-depth comparisons are made with available experimental data.

2. Problem Descriptions

Fig. 1 shows a vertical riser subject to VIV in uniform currents. The flow direction is parallel to the global *x* axis. A top tension *T* is applied to the top end of the riser. The riser is pinned at both ends and free to move in the in-line (*x*) and cross-flow (*y*) directions. In order to make a reasonable comparison, all the parameters are kept the same as Tognarelli et al. (2004). Detailed information about the riser is summarised in Table 1.

Properties	Values	SI units
L	9.63	m
D_o	20	mm
t	0.45	mm
E	1.025×10^{11}	N/m^2
T	817	N
*m**	2.23	-
L/D	481.5	-

Table 1 Properties of the model riser.

3. Numerical Methods

ANSYS MFX solver is adopted to solve the FSI problem in this paper.

3.1 Flow Model

The fluid flow around the riser is modelled by solving the unsteady, incompressible Navier-Stokes equations. The turbulence flow is simulated using large eddy simulation (LES) wall-adapted local eddy-viscosity (WALE) model (Nicoud and Ducros, 1999).

The filtered Navier-Stokes equations are as follows.

$$\frac{\partial \bar{u}_i}{\partial x_i} = 0 \tag{1}$$

$$\frac{\partial \bar{u}_i}{\partial t} + \frac{\partial}{\partial x_j}\left(\bar{u}_i \bar{u}_j\right) = -\frac{\partial \bar{p}}{\partial x_i} + \frac{\partial}{\partial x_j}\left[\nu\left(\frac{\partial \bar{u}_i}{\partial x_j} + \frac{\partial \bar{u}_j}{\partial x_i}\right)\right] - \frac{\partial \tau_{ij}}{\partial x_j} \tag{2}$$

where τ_{ij} denotes the subgrid-scale stress. It is defined by

$$\tau_{ij} = \overline{u_i u_j} - \bar{u}_i \bar{u}_j \tag{3}$$

The subgrid-scale stress τ_{ij} is related to the large-scale strain rate tensor $\bar{S}_{ij}$ by Boussinesq approximation:

$$-\left(\tau_{ij} - \frac{\delta_{ij}}{3}\tau_{kk}\right) = 2\nu_{sgs}\bar{S}_{ij} \tag{4}$$

$$\bar{S}_{ij} = \frac{1}{2}\left(\frac{\partial \bar{u}_i}{\partial x_j} + \frac{\partial \bar{u}_j}{\partial x_i}\right) \tag{5}$$

The eddy-viscosity is computed by

$$\nu_{sgs} = \left(C_w \Delta\right)^2 \frac{\left(S_{ij}^d S_{ij}^d\right)^{3/2}}{\left(\bar{S}_{ij}\bar{S}_{ij}\right)^{5/2} + \left(S_{ij}^d S_{ij}^d\right)^{5/4}} \tag{6}$$

where S_{ij}^d denotes the traceless symmetric part of the square of the velocity gradient tensor:

$$S_{ij}^d = \frac{1}{2}\left(\bar{g}_{ij}^2 + \bar{g}_{ji}^2\right) - \frac{1}{3}\delta_{ij}\bar{g}_{kk}^2 \tag{7}$$

where $\bar{g}_{ij}^2 = \bar{g}_{ik}\bar{g}_{kj}$, $\bar{g}_{ij} = \partial \bar{u}_i / \partial x_j$ and δ_{ij} is the Kronecker symbol. The tensor S_{ij}^d can be rewritten in terms of the strain-rate and vorticity tensors:

$$S_{ij}^{d} = \bar{S}_{ik}\bar{S}_{kj} + \bar{\Omega}_{ik}\bar{\Omega}_{kj} - \frac{1}{3}\delta_{ij}\left(\bar{S}_{mn}\bar{S}_{mn} - \bar{\Omega}_{mn}\bar{\Omega}_{mn}\right) \quad (8)$$

where the vorticity tensor is given by

$$\bar{\Omega}_{ij} = \frac{1}{2}\left(\frac{\partial \bar{u}_i}{\partial x_j} - \frac{\partial \bar{u}_j}{\partial x_i}\right) \quad (9)$$

The main advantages of the WALE model are the capability to reproduce the laminar to turbulent transition and the design of the model to return the correct wall-asymptotic y^{+3} (ANSYS Inc., 2013)

The governing equations are discretised using element-based finite volume method (FVM). Rhie-Chow interpolation is used for pressure velocity coupling. A second-order backward Euler scheme is applied for temporal discretisation and a bounded central difference scheme is adopted for the convective term.

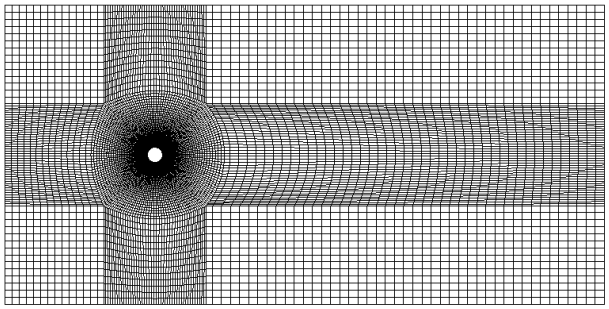

Fig. 2 Mesh at *z/L* = constant.

Fig. 2 shows the computational mesh in the *x*-*y* plane. A Dirichlet boundary condition is applied to the inlet. A Neumann boundary condition is imposed on the outlet. A no-slip boundary condition is used on the cylinder surface and other surfaces are modelled as symmetry planes where the velocity normal to the symmetry boundary is zero and the scalar variable gradients normal to the boundary are also zero.

3.2 Structural Dynamic Model

The governing equation of a structure's motion is given by

$$[M]\{\ddot{u}\} + [C]\{\dot{u}\} + [K]\{u\} = \{F\} \quad (10)$$

where $\{u\}$ is the nodal displacement vector and a dot denotes differentiation with respect to time. $[M]$, $[C]$ and $[K]$ are the mass, damping and stiffness matrices, respectively. $\{F\}$ is the hydrodynamic force vector. It is solved using the Hilber-Hughes-Taylor (HHT) method (Chung and Hulbert, 1993) with a second order accuracy.

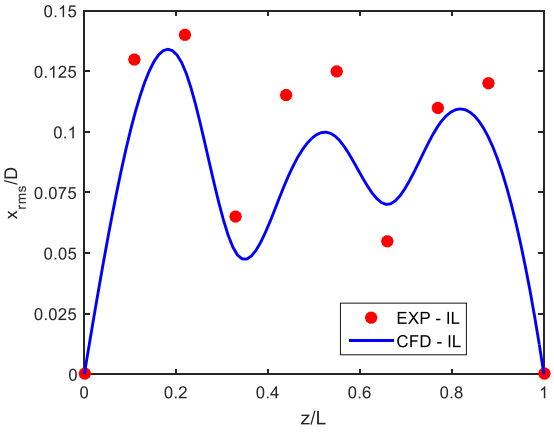

(a)

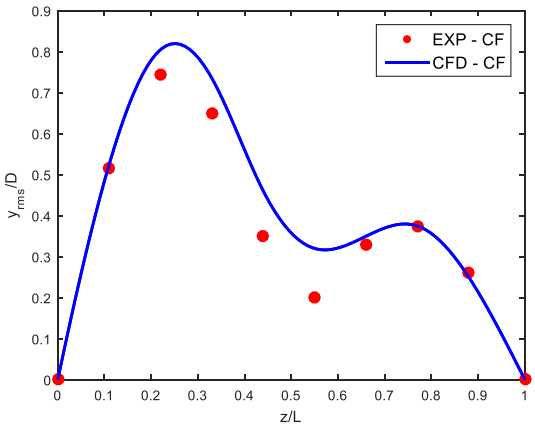

(b)

Fig. 3 Comparison of CF and IL amplitudes: (a) IL rms amplitude and (b) CF rms amplitude.

4. VIV of a Vertical Riser in Uniform Flow

VIV responses of a vertical riser immersed in uniform currents are analysed. The current speed is U = 0.42 m/s. The Reynolds number for U = 0.42 m/s is 7381.

Fig. 3 shows the comparison of the in-line (IL) and cross-flow (CF) amplitudes. The CFD results are in good agreement with the experimental results. The predicted IL and CF root mean square (rms) amplitudes are x_{rms}/D = 0.13 and y_{rms}/D = 0.8, respectively.

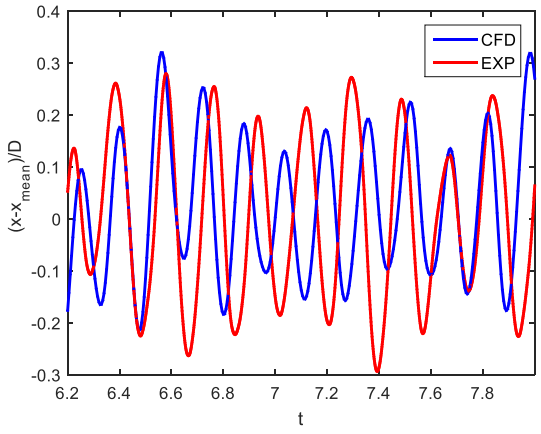

(a)

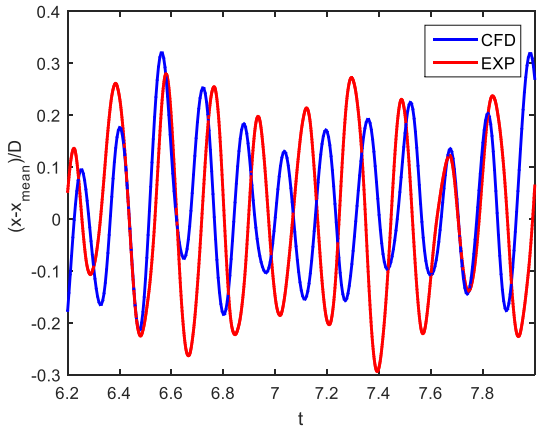

(b)

Fig. 4 Time history of displacements (a) IL and (b) CF.

The time history of IL and CF displacements at z/L = 0.22 is compared to the experimental results in Fig. 4. The predicted amplitudes and frequencies agree with those obtained in the experiment.

The combined in-line and transverse vibrations of a single cylinder typically present a figure-of-eight motion as the dominant frequency in the drag fluctuation is twice of that in the lift (Prasanth and Mittal, 2009). A figure-of-eight trajectory is also observed in the present simulation, but different from the highly repeatable figure-of-eight shapes obtained from low Reynolds number laminar flow simulations, the trajectory in the present simulation exhibits a nonrepeatable feature. Dahl et al. (2010) attributed this nonrepeatability at subcritical Reynolds numbers to the irregular in-line motion. Nevertheless, the orbital trajectories predicted by the current CFD simulation are in accordance with those in the experiment. An example of orbital trajectory at z/L = 0.22 is given in Fig. 5. The path direction of the cylinder motion at z/L = 0.22 appears to have a clockwise trajectory which illustrates the direction of the cylinder's motion at the top position of the figure-of-eight path. According to the previous study by Bourguet et al. (2011), clockwise orbits are associated with damping fluid forces.

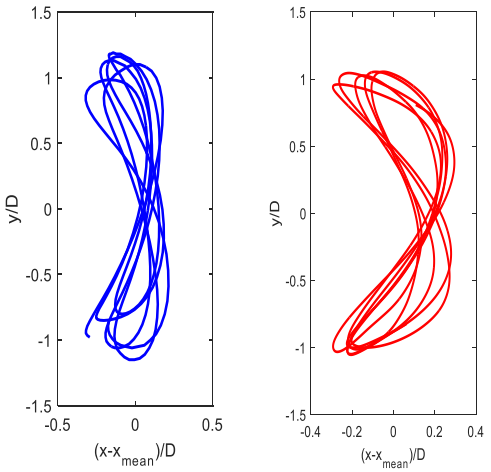

(a) (b)

Fig. 5 Orbital trajectory at z/L = 0.22: (a) CFD and (b) EXP.

The oscillation frequencies of the cylinder at z/L = 0.22 predicted by CFD is given in Fig. 6. The power spectral density (PSD) of IL and CF responses are plotted against the frequency. From the PSD plots, the IL oscillation frequency is f_{ox} = 6.484 Hz and the CF oscillation frequency is f_{oy} = 2.993 Hz. The ratio of IL to CF oscillation frequency is around 2 which verifies the occurrence of dual resonance.

Fig. 7 presents the z-vorticity at different sections of the riser when t = 8 s. 2P mode is observed at z/L = 0.3 where the largest transverse vibration amplitude is found ($y_{max}/D \approx$ 1) whereas 2S mode is observed elsewhere along the riser.

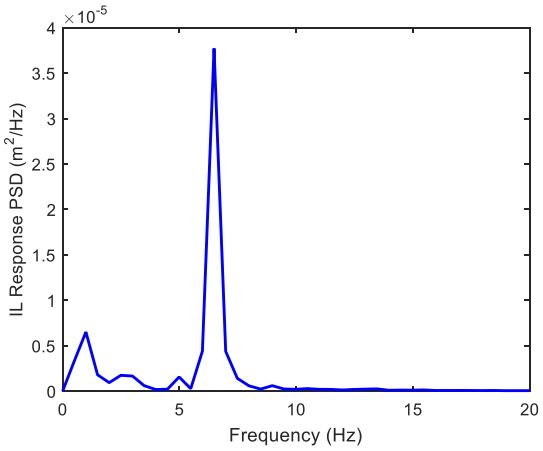

(a)

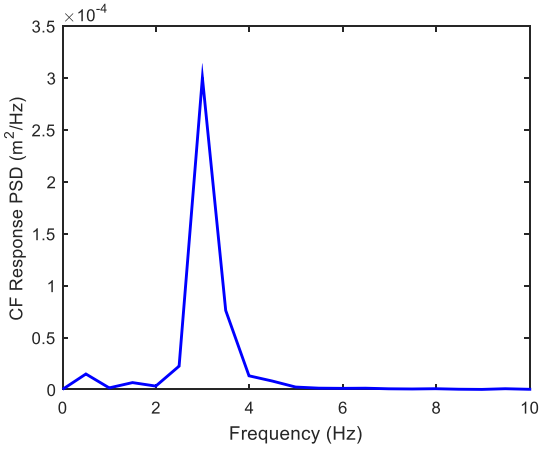

(b)

Fig. 6 Response PSD: (a) IL and (b) CF.

5. Conclusions

VIV response of a riser was studied using 3D LES. Simulation results of uniform flow with U = 0.42 m/s were presented. The CFD results are in good agreement with the published experimental data which shows that the present 3D CFD method is capable of predicting VIV of long risers. The following conclusions can be reached.

The displacement along the riser agree with experimental data in both the IL and CF directions. When the riser model is exposed to a flow with free-stream velocity U = 0.42 m/s, the riser vibrate in the 3rd and the 2nd modes in the IL and CF directions, respectively. The IL rms amplitude is x_{rms}/D = 0.13 and the CF rms amplitude is y_{rms}/D = 0.8.

The motion trajectory of the riser is of a figure-of-eight shape and the ratio of the IL to CF oscillation frequency is around 2. Both results indicate the occurrence of dual resonance.

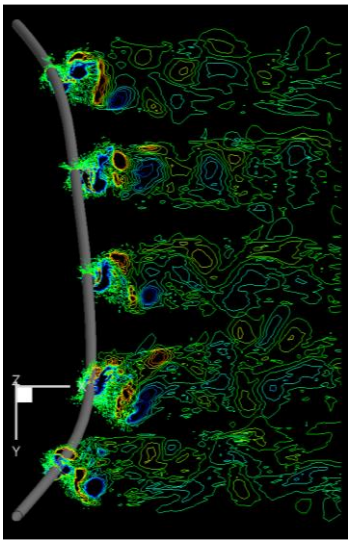

Fig. 7 Z-vorticity along the span at t = 8 s.

2P vortex shedding mode is observed at the location corresponds to the largest transverse amplitude. 2S mode is observed elsewhere along the riser.

Acknowledgement

Results are obtained using the EPSRC funded ARCHIE-WeSt High Performance Computer (www.archie-west.ac.uk). EPSRC grant no. EP/K000586/1. The authors are also grateful to the “Faculty Engineering Technology Studentship” jointly funded by the Faculty of Engineering and the Department of Naval Architecture, Ocean and Marine Engineering.

References

ANSYS Inc., 2013. ANSYS CFX-Solver Theory Guid, Canonsburg, USA.

Bearman, P.W., 1984. Vortex shedding from oscillating bluff body. Annu. Rev. Fluid Mech. 16, 195-222.

Bearman, P.W., 2011. Circular cylinder wakes and vortex-induced vibrations. J. Fluids Struct. 27, 648-658.

Bourguet, R., Modarres-Sadeghi, Y., Karniadakis, G.E., Triantafyllou, M.S., 2011. Wake-body resonance of long flexible structures is dominated by counterclockwise orbits. Phys. Rev. Lett. 107.134502, 1-4.

Chaplin, J.R., Bearman, P.W., Huera Huarte, F.J., Pattenden, R.J., 2005. Laboratory measurement of vortex-induced vibrations of a vertical tension riser in a stepped current. J. Fluids Struct. 21, 3-24.

Chung, J., Hulbert, G.M., 1993. A time integration algorithm for structural dynamics with improved numerical dissipation: the generalised - α method. J. Appl. Mech. 60, 371-375.

Constantinides, H., Oakley, O.H., 2008a. Assessment of emprical VIV analysis tools and benchmark with experiments, OMAE2008-57216, Proc. 27th OMAE Conf., Estoril, Portugal.

Constantinides, Y., Oakley, O.H., 2008b. Numerical prediction of VIV and comparison with field experiments, OMAE2008-57215, Proc. 27th OMAE Conf., Estoril, Portugal.

Dahl, J.M., Hover, F.S., Triantafyllou, M.S., Oakley, O.H., 2010. Dual resonance in vortex-induced vibrations at subcritical Reynolds numbers. J. Fluid Mech. 643, 395-424.

Gabbai, R.D., Benaroya, H., 2005. An overview of modelling and experiments of vortex-induced vibrations of circular cylinders. J. Sound Vib. 282, 575-616.

Gu, J., Vitola, M., Coelho, J., Pinto, W., Duan, M., Levi, C., 2013. An experimental investigation by towing tank on VIV of a long flexible cylinder for deepwater riser application. J. Mar. Sci. Technol. 18, 358-369.

Holmes, S., Oakley, O.H., Constantinides, H., 2006. Simulation of riser VIV using fully three dimensional CFD simulations, OMAE2006-92124, Proc. 25th OMAE Conf., Hamburg, Germany.

Huang, K., Chen, H.C., Chen, C.R., 2009. Vertical riser VIV simulation in uniform current. J. Offshore Mech. Arct. Eng. 132, 1-10.

Meneghini, J.R., Saltara, F., Fregonesi, R.A., Yamamoto, C.T., Casaprima, E., Ferrari, J.A., 2004. Numerical simulation of VIV on long flexible cylinders immersed in complex flow fields. Eur. J. Mech. B/Fluids 23, 51-63.

Menter, F., Sharkey, P., Yakubov, S., Kuntz, M., 2006. Overview of fluid-structure coupling in ANSYS-CFX, OMAE2006-92145, Proc. 25th OMAE Conf., Hamburg, Germany.

Nicoud, F., Ducros, F., 1999. Subgrid-scale stress modelling based on the square of the velocity gradient tensor. Flow Turbul. Combust. 62, 183-200.

Prasanth, T.K., Mittal, S., 2009. Vortex-induced vibration of two circular cylinders at low Reynolds number. J. Fluids Struct. 25, 731-741.

Sarpkaya, T., 1979. Vortex-induced oscillations. J. Appl. Mech. 46 (241-258).

Tognarelli, M.A., Slocum, S.T., Frank, W.R., Campbell, R.B., 2004. VIV response of a long flexible cylinder in uniform and linearly sheared currents, OTC 16338, Proc. 2004 Offshore Tech. Conf., Houston, Texas, USA.

Tognarelli, M.A., Taggart, S., Campbell, M., 2008. Actual VIV fatigue response of full scale drilling risers: with and without suppression devices, OMAE2008-57046, Proc. 27th OMAE Conf., Estoril, Portugal.

Trim, A.D., Braaten, H., Lie, H., Tognarelli, M.A., 2005. Experimental investigation of vortex-induced vibration of long marine risers. J. Fluids Struct. 21, 335-361.

Vandiver, J.K., Swithenbank, S., Jaiswal, V., Marcollo, H., 2006. The effectiveness of helical strakes in the suppression of high-mode-number VIV, OTC 18276, Proc. 2006 Offshore Tech. Conf., Houston, Texas, USA.

Willden, R.H.J., Graham, J.M.R., 2001. Numerical prediction of VIV on long flexible circular cylinders. J. Fluids Struct. 15, 659-669.

Williamson, C.H.K., Govardhan, R., 2004. Vortex-induced vibrations. Annu. Rev. Fluid Mech. 36, 413-455.

Yamamoto, C.T., Meneghini, J.R., Saltara, F., Fregonesi, R.A., Ferrari, J.A., 2004. Numerical simulations of vortex-induced vibration on flexible cylinders. J. Fluids Struct. 19, 467-489.